Inorganic Chemistry

Article

pubs.acs.org/IC

Series of Inorganic–Organic Hybrid Materials Constructed From Octamolybdates and Metal–Organic Frameworks: Syntheses, Structures, and Physical Properties

Wei-Qiu Kan, Jin Yang,* Ying-Ying Liu, and Jian-Fang Ma*

Key Lab of Polyoxometalate Science, Department of Chemistry, Northeast Normal University, Changchun 130024, People's Republic of China

Supporting Information

ABSTRACT: Series of inorganic–organic hybrid materials based on octamolybdates, silver ions, and multidentate N-donor ligands, namely, $[Ag_2(2,3'\text{-tmbpt})(\beta\text{-}Mo_8O_{26})_{0.5}]$ (**1**), $[Ag_2(2,4'\text{-tmbpt})_2(\alpha\text{-}Mo_8O_{26})_{0.5}(H_2O)_{0.5}]\cdot 2H_2O$ (**2**), $[Ag_3(3,3'\text{-tmbpt})_2(\alpha\text{-}H_2Mo_8O_{26})_{0.5}(\beta\text{-}Mo_8O_{26})_{0.5}]\cdot 3.5H_2O$ (**3**), $[Ag_2(3,3'\text{-tmbpt})(\varepsilon\text{-}Mo_8O_{26})_{0.5}]\cdot 1.75H_2O$ (**4**), $[Ag_2(3,4'\text{-tmbpt})_2(\beta\text{-}Mo_8O_{26})_{0.5}]\cdot 0.5H_2O$ (**5**), and $[Ag(3,4'\text{-Htmbpt})(\beta\text{-}Mo_8O_{26})_{0.5}]$ (**6**), where 2,3′-tmbpt = 1-((1H-1,2,4-triazol-1-yl)methyl)-3-(3-pyridyl)-5-(2-pyridyl)-1,2,4-triazole), 2,4′-tmbpt = 1-((1H-1,2,4-triazol-1-yl)methyl)-3-(4-pyridyl)-5-(2-pyridyl)-1,2,4-triazole), 3,3′-tmbpt = 1-((1H-1,2,4-triazol-1-yl)methyl)-3,5-bis(3-pyridyl)-1,2,4-triazole, and 3,4′-tmbpt = 1-((1H-1,2,4-triazol-1-yl)methyl)-3-(4-pyridyl)-5-(3-pyridyl)-1,2,4-triazole) have been synthesized under hydrothermal conditions. Compound **1** displays a rare 3D (3,4,8)-connected net with $(4\cdot8^2)(4^2\cdot8^4)(4^3\cdot8^{20}\cdot10^5)$ topology. Compound **2** shows a rare 3D (4,6)-connected self-catenated framework with $(6^4\cdot8^2)(4^2\cdot6^3\cdot8^2)(4^2\cdot6^8\cdot8^4\cdot10)$ topology. Compound **3** is a scarce 3D framework based on two different kinds of $[Mo_8O_{26}]^{4-}$ isomers. Compound **4** exhibits a 3D framework constructed by silver–organic sheets and the rare $[\varepsilon\text{-}Mo_8O_{26}]^{4-}$ anions. Compound **5** shows an interesting 1D → 2D polythreaded structure. Compound **6** displays a 2D layer structure, which is further linked by the N–H···O hydrogen bonds to form a 3D supramolecular architecture. Their structures have been further characterized by infrared spectra (IR), elemental analyses, powder X-ray diffraction (PXRD), electrochemistry and photoluminesce. Moreover, the photocatalytic activities for degradation of organic pollutant have been investigated for compounds **3**–**6**.

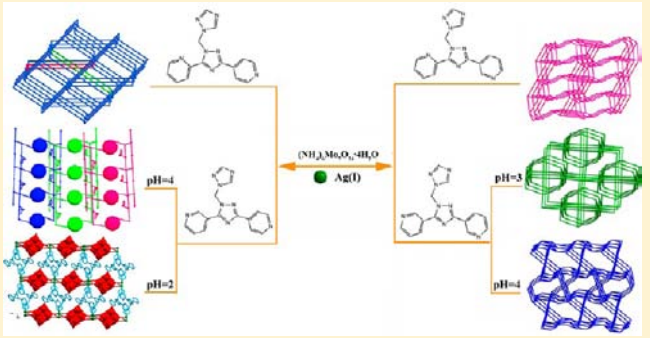

INTRODUCTION

Polyoxometalates (POMs), as one kind of significant metal oxide cluster with controllable shape and size, highly negative charges, and oxo-enriched surfaces, are good candidates in the design and synthesis of new functional inorganic–organic hybrid materials.[1,2] Among the various types of POMs, the octamolybdate (Mo_8) has attracted much attention because of its high reactivities and diverse isomers.[3] So far, eight isomeric forms of octamolybdates have been prepared (α, β, γ, δ, ε, ζ, η, and θ isomers), which can be distinguished from each other by the different numbers of $[MoO_4]$, $[MoO_5]$, and $[MoO_6]$ units.[4] These isomers can afford plenty of oxygen atoms and display a variety of structural patterns with different sizes, so they can act as excellent multidentate inorganic building blocks for the construction of functional inorganic–organic hybrid materials.[5] Meanwhile, $\{Mo_8\}$ clusters can be easily made from $(NH_4)_6Mo_7O_{24}\cdot 4H_2O$ under hydrothermal conditions with controlled pH values.[2b,5]

However, the organic ligands play an important role in controlling and adjusting the topologies and physical properties of inorganic–organic hybrid materials. In this regard, the multidentate N-donor ligands tmbpt (1-((1H-1,2,4-triazol-1-yl)methyl)-3,5-bis(pyridyl)-1,2,4-triazole) (Scheme 1) are excellent candidates for the construction of inorganic–organic hybrid materials with intriguing structures for the following reasons: (i) the two pyridyl and two triazolyl groups can provide multiple coordination sites and adopt versatile coordination modes, (ii) the flexible $-CH_2-$ spacer allows the triazolyl group to bend and rotate freely for conforming to the coordination geometries of metal ions. Moreover, POM-based inorganic–organic hybrid materials containing silver ions often show relatively high catalytic activity for degradation of dye when used as catalysts due to the synergistic effect between the silver-organic fragments and POMs.[6]

In this work, series of inorganic–organic hybrid materials based on octamolybdates, silver ions and tmbpt ligands, namely, $[Ag_2(2,3'\text{-tmbpt})(\beta\text{-}Mo_8O_{26})_{0.5}]$ (**1**), $[Ag_2(2,4'\text{-tmbpt})_2(\alpha\text{-}Mo_8O_{26})_{0.5}(H_2O)_{0.5}]\cdot 2H_2O$ (**2**), $[Ag_3(3,3'\text{-tmbpt})_2(\alpha\text{-}H_2Mo_8O_{26})_{0.5}(\beta\text{-}Mo_8O_{26})_{0.5}]\cdot 3.5H_2O$ (**3**),

Received: January 18, 2012
Published: October 22, 2012

Scheme 1. Tmbpt Ligands Used in This Work

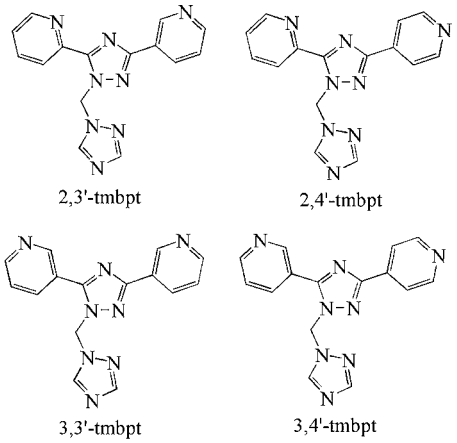

$[Ag_2(3,3'\text{-tmbpt})(\varepsilon\text{-}Mo_8O_{26})_{0.5}]\cdot 1.75H_2O$ (**4**), $[Ag_2(3,4'\text{-tmbpt})_2(\beta\text{-}Mo_8O_{26})_{0.5}]\cdot 0.5H_2O$ (**5**), and $[Ag(3,4'\text{-Htmbpt})(\beta\text{-}Mo_8O_{26})_{0.5}]$ (**6**), where 2,3′-tmbpt = 1-((1H-1,2,4-triazol-1-yl)methyl)-3-(3-pyridyl)-5-(2-pyridyl)-1,2,4-triazole), 2,4′-tmbpt = 1-((1H-1,2,4-triazol-1-yl)methyl)-3-(4-pyridyl)-5-(2-pyridyl)-1,2,4-triazole), 3,3′-tmbpt = 1-((1H-1,2,4-triazol-1-yl)methyl)-3,5-bis(3-pyridyl)-1,2,4-triazole, and 3,4′-tmbpt = 1-((1H-1,2,4-triazol-1-yl)methyl)-3-(4-pyridyl)-5-(3-pyridyl)-1,2,4-triazole) have been successfully synthesized under hydrothermal conditions. Their optical band gaps, photoluminescent properties, electrochemistry, and the photocatalytic behaviors have been described in detail.

EXPERIMENTAL SECTION

Materials and Methods. The tmbpt ligands were prepared by the procedures reported.[7] Other reagents were obtained commercially and used without further purification. Elemental analyses were carried out with a PerkinElmer 240 elemental analyzer. The FTIR spectra were recorded from KBr pellets in the range of 4000−400 cm^{-1} on a Mattson Alpha-Centauri spectrometer. The solid-state photoluminescent spectra were recorded on a FLSP920 Edinburgh Fluorescence Spectrometer at room temperature. Diffuse reflectivity spectra were collected on a finely ground sample with a Cary 500 spectrophotometer equipped with a 110 mm diameter integrating sphere, which were measured from 200 to 800 nm. PXRD patterns of the samples were recorded on a Rigaku Dmax 2000 X-ray diffractometer with graphite monochromatized Cu−Kα radiation (λ = 0.154 nm) and 2θ varying from 5 to 50°. The experimental PXRD patterns are in good agreement with the corresponding simulated ones (Figure S1 of the Supporting Information). The photocatalytic activities were tested by a 756 CRT UV−vis spectrophotometer. Electrochemical measurements were performed with a CHI660b electrochemical workstation. A conventional three-electrode system was used. Ag/AgCl (3 M KCl) electrode was used as a reference electrode, and a Pt wire as a counter electrode. Chemically bulk-modified carbon-paste electrode (CPEs) was used as the working electrode. Photocatalytic experiments were performed in conventional processes. A suspension containing compounds **3**−**6** (70 mg) and 200 mL methylene blue (MB) (5×10^{-5} mol L^{-1}) aqueous solution was stirred in the dark for about 30 min in order to reach adsorption−desorption equilibrium between the photocatalyst and MB. It was then stirred under a 125 W Hg lamp. At 15 min intervals, 3 mL of samples were taken out of the reactor and separated by centrifuge to remove suspended catalyst particles and then subjected to spectroscopic measurement on the UV−vis spectrometer. The concentration of MB was estimated by the absorbance at 665 nm, which directly relates to the structure change of its chromophore. The Brunauer−Emmett−Teller (BET) specific surface areas (S_{BET}) of the powders of compounds **3**−**6** were measured on an ASAP 2020 nitrogen adsorption apparatus.

*Synthesis of $[Ag_2(2,3'\text{-tmbpt})(\beta\text{-}Mo_8O_{26})_{0.5}]$ (**1**).* A mixture of 2,3′-tmbpt (0.03 g, 0.1 mmol), $AgNO_3$ (0.102 g, 0.6 mmol), $(NH_4)_6Mo_7O_{24}\cdot 4H_2O$ (0.37 g, 0.3 mmol), and water (8 mL) was placed in a Teflon reactor (15 mL) and heated at 130 °C for 3 days. After cooling to room temperature at a rate of 10 °C·h^{-1}, colorless crystals of **1** were collected in 7% yield. The initial and final pH values of the reaction system were about 5 and 5.5, respectively. Anal. Calcd for $C_{15}H_{12}Ag_2Mo_4N_8O_{13}$ (M_r = 1111.83): C, 16.20; H, 1.09; N, 10.10. Found: C, 16.12; H, 1.02; N, 10.19. IR (KBr, cm^{-1}): 3423(w), 3143(w), 1638(w), 1595(w), 1511(w), 1456(w), 1420(w), 1364(w), 1273(w), 1199(w), 1139(w), 1093(w), 1009 (w), 983(s), 889(s), 825(s), 747(w), 708(s), 691(s), 678(s), 560(m), 522(m).

*Synthesis of $[Ag_2(2,4'\text{-tmbpt})_2(\alpha\text{-}Mo_8O_{26})_{0.5}(H_2O)_{0.5}]\cdot 2H_2O$ (**2**).* The preparation of **2** was similar to that of **1** except that 2,4′-tmbpt (0.03 g, 0.1 mmol) was used instead of 2,3′-tmbpt. Colorless crystals of **1** were collected in 21% yield. The initial and final pH values of the reaction system were about 5 and 5.5, respectively. Anal. Calcd for $C_{60}H_{58}Ag_4Mo_8N_{32}O_{31}$ (M_r = 2922.38): C, 24.66; H, 2.00; N, 15.34. Found: C, 24.57; H, 2.05; N, 15.44. IR (KBr, cm^{-1}): 3196 (w), 3092(w), 1638(w), 1618(w), 1587(w), 1510 (w), 1456(w), 1419(w), 1365(w), 1322(w), 1275(w), 1200(w), 1139(w), 1011(w), 949(s), 889(s), 833(s), 750(m), 692(s), 653(s), 569(m), 519(m).

*Synthesis of $[Ag_3(3,3'\text{-tmbpt})_2(\alpha\text{-}H_2Mo_8O_{26})_{0.5}(\beta\text{-}Mo_8O_{26})_{0.5}]\cdot 3.5H_2O$ (**3**).* The preparation of **3** was similar to that of **2** except that 3,3′-tmbpt (0.03 g, 0.1 mmol) was used instead of 2,4′-tmbpt and the pH value was adjusted to about 3. Colorless crystals of **3** were collected in 57% yield. The final pH value of the reaction system was about 5. Anal. Calcd for $C_{30}H_{31}Ag_3Mo_8N_{16}O_{29.5}$ (M_r = 2178.84): C, 16.54; H, 1.44; N, 10.29. Found: C, 16.51; H, 1.49; N, 10.43. IR (KBr, cm^{-1}): 3423 (w), 3129(w), 3041(w), 1604(w), 1588(w), 1533(w), 1512(w), 1465(w), 1453(w), 1427(m), 1380(m), 1308(w), 1283(w), 1245(w), 1209(w), 1138(m), 1041(w), 1016(w), 995(w), 944(s), 925(s), 898(s), 840(s), 814(w), 767(w), 700(m), 665(s), 559(w), 524(w).

*Synthesis of $[Ag_2(3,3'\text{-tmbpt})(\varepsilon\text{-}Mo_8O_{26})_{0.5}]\cdot 1.75H_2O$ (**4**).* The preparation of **4** was similar to that of **3** except that the pH value was adjusted to about 4. Colorless crystals of **4** were collected in 42% yield. The final pH value of the reaction system was about 4.5. Anal. Calcd for $C_{15}H_{13.5}Ag_2Mo_4N_8O_{14.75}$ (M_r = 1141.34): C, 15.78; H, 1.19; N, 9.82. Found: C, 15.71; H, 1.10; N, 9.95. IR (KBr, cm^{-1}): 3443(w), 3129(w), 3068(w), 1604(w), 1587(w), 1534(w), 1453(w), 1426(w), 1380(w), 1353(w), 1308(w), 1281(w), 1245(w), 1209(w), 1138(w), 1044(w), 1030(w), 944(s), 898(s), 839(s), 815(w), 803(w), 767(w), 700(m), 664(s), 559(w), 522(w).

*Synthesis of $[Ag_2(3,4'\text{-tmbpt})_2(\beta\text{-}Mo_8O_{26})_{0.5}]\cdot 0.5H_2O$ (**5**).* The preparation of **5** was similar to that of **4** except that 3,4′-tmbpt (0.03 g, 0.1 mmol) was used instead of 3,3′-tmbpt. Colorless crystals of **5** were collected in 32% yield. The final pH value of the reaction system was about 4.5. Anal. Calcd for $C_{30}H_{25}Ag_2Mo_4N_{16}O_{13.5}$ (M_r = 1425.16): C, 25.18; H, 1.77; N, 15.73. Found: C, 25.11; H, 1.82; N, 15.63. IR (KBr, cm^{-1}): 3444(w), 3105(w), 1615(w), 1507(w), 1418(w), 1305(w), 1269(w), 1205(w), 1133(w), 1017(w), 945(s), 892(s), 840(m), 720(m), 698(m), 650(s), 583(s), 513(s).

*Synthesis of $[Ag(3,4'\text{-Htmbpt})(\beta\text{-}Mo_8O_{26})_{0.5}]$ (**6**).* The preparation of **6** was similar to that of **5** except that the pH value was adjusted to about 2. Colorless crystals of **6** were collected in 39% yield. The final pH value of the reaction system was about 4. Anal. Calcd for $C_{15}H_{13}AgMo_4N_8O_{13}$ (M_r = 1004.96): C, 17.93; H, 1.31; N, 11.15. Found: C, 17.88; H, 1.22; N, 11.03. IR (KBr, cm^{-1}): 3444(w), 3007(w), 1621(w), 1603(w), 1558(w), 1516(w), 1433(w), 1302(w), 1240(w), 1208(w), 1132(w), 1024(w), 934(s), 888(s), 847(m), 738(s), 671(s), 653(s), 553(w), 519(w).

X-ray Crystallography. Single-crystal X-ray diffraction data for compounds **1**-**6** were recorded on an Oxford Diffraction Gemini R Ultra diffractometer with graphite-monochromated Mo Kα radiation (λ = 0.71073 Å) at 293 K. Absorption corrections were performed using multiscan technique. The structures were solved by Direct Method of *SHELXS-97*[8a] and refined by full-matrix least-squares techniques using the *SHELXL-97* program.[8b] Non-hydrogen atoms of the compounds were refined with anisotropic temperature parameters.

dx.doi.org/10.1021/ic300134z | Inorg. Chem. 2012, 51, 11266−11278

All hydrogen atoms on carbon and nitrogen atoms were generated geometrically and refined using a riding model with d(C−H) = 0.93 Å, d(N−H) = 0.86 Å, U_{iso} = 1.2U_{eq}(C, N) for aromatic and d(C−H) = 0.97 Å, U_{iso} = 1.2U_{eq}(C) for CH_2 atoms. The disordered atoms O1W for **2** and Mo6 for **3** were refined using the atoms split over two sites with a total occupancy of 0.5 and 1, respectively. Hydrogen atoms of water molecules for **2**−**5** were not included in the model. The detailed crystallographic data and structure refinement parameters of compounds **1**−**6** are summarized in Table 1. Selected bond distances, angles for them are listed in Tables S1−S6 of the Supporting Information. The maximum residual electron density is 1.58 eÅ $^{-3}$ at 0.9 Å from Mo3 for compound **2**, 1.10 eÅ $^{-3}$ at 0.9 Å from Ag2 for compound **3**, and 1.82 eÅ $^{-3}$ at 0.9 Å, and 1.06 eÅ $^{-3}$ at 0.6 Å from Ag2 for compound **5**. These residual electron densities near heavy atom sites can be interpreted as Fourier truncation errors.[9]

RESULTS AND DISCUSSION

To check the oxidation state of Mo atoms and protonation states (O, OH, or H_2O) of oxygen sites, the bond valence sum calculations were carried out for compounds **1**−**6**.[10] The calculated result reveals that the average oxidation state of Mo atoms in compounds **1**−**6** is +VI. Therefore, the Mo_8O_{26} anions in compounds **1**−**6** display −IV valence.

Structure of [Ag$_2$(2,3′-tmbpt)(β-Mo$_8$O$_{26}$)$_{0.5}$] (1). The asymmetric unit of **1** consists of two Ag(I) ions, one 2,3′-tmbpt ligand, and half a [β-Mo_8O_{26}]$^{4-}$ anion. The [Mo_8O_{26}]$^{4-}$ cluster, which is built from eight distorted MoO_6 edge-shared octahedra, is a typical β-octamolybdate.[11] As shown in part a of Figure 1, both Ag1 and Ag2 are five-coordinated in trigonal biyramid coordination geometries, but their coordination environments are entirely different. Ag1 is coordinated by one nitrogen atom from one 2,3′-tmbpt ligand and four terminal oxygen atoms from two different [β-Mo_8O_{26}]$^{4-}$ anions. Ag2 is coordinated by two nitrogen atoms from two individual 2,3′-tmbpt ligands and three terminal oxygen atoms from two distinct [β-Mo_8O_{26}]$^{4-}$ anions. The Ag−N bond lengths range from 2.197(4) to 2.208(4) Å and the Ag−O bond distances are in the range of 2.254(3)-2.857(4) Å. All of these bond lengths are within the normal ranges observed in other Ag(I)-containing complexes.[12] In **1**, each [β-Mo_8O_{26}]$^{4-}$ anion coordinates to eight Ag(I) ions to generate a 2D layer (part b of Figure 1). The 2,3′-tmbpt ligands, act as tridentate ligands, further bridge the layers to yield a complicate 3D framework (part c of Figure 1).

Topologically, the Ag1 ions and the 2,3′-tmbpt ligands can be considered as 3-connected nodes, the Ag2 ions can be viewed as 4-connected nodes and the [β-Mo_8O_{26}]$^{4-}$ anions can be reduced to 8-connected nodes. Thus, the whole 3D framework can be simplified as a (3,4,8)-connected net with $(4{\cdot}8^2)(4^2{\cdot}8^4)(4^3{\cdot}8^{20}{\cdot}10^5)$ topology (part d of Figure 1). Up to now, thousands of inorganic−organic hybrid materials have been reported, but highly connected (≥8) ones assembled from POMs are exceedingly rare.[13] Compound **1** represents an unprecedented (3,4,8)-connected topological framework assembled from octamolybdate.

Structure of [Ag$_2$(2,4′-tmbpt)$_2$(α-Mo$_8$O$_{26}$)$_{0.5}$(H$_2$O)$_{0.5}$]·2H$_2$O (2). The asymmetric unit of **2** contains two Ag(I) ions, two 2,4′-tmbpt ligands, half a [α-Mo_8O_{26}]$^{4-}$ anion and two and a half water molecules. Each [α-Mo_8O_{26}]$^{4-}$ anion consists of a ring of six edge-sharing {MoO_6} octahedra capped at the poles by two {MoO_4} tetrahedra.[11a,14] As shown in part a of Figure 2, Ag1 and Ag3 are four-coordinated in square planar coordination geometries, but their coordination environments are different. Ag1 is coordinated by two nitrogen atoms from two individual 2,4′-tmbpt ligands and two terminal oxygen atoms from two distinct [α-Mo_8O_{26}]$^{4-}$ anions. Ag3 is coordinated by two nitrogen atoms from two different 2,4′-tmbpt ligands and two oxygen atoms from two water

Table 1. Crystal Data and Structure Refinements for Compounds 1−6[a,b]

	1	2
formula	$C_{15}H_{12}Ag_2Mo_4N_8O_{13}$	$C_{60}H_{58}Ag_4Mo_8N_{32}O_{31}$
fw	1111.83	2922.38
cryst syst	triclinic	triclinic
space group	*P*-1	*P*-1
a (Å)	9.960(5)	11.795(5)
b (Å)	10.842(5)	13.564(5)
c (Å)	12.121(5)	16.478(5)
α (°)	77.350(5)	68.809(5)
β (°)	84.755(5)	70.639(5)
γ (°)	84.329(5)	84.471(5)
V (Å^3)	1267.6(10)	2318.2(15)
Z	2	1
D_c (g/cm^{-3})	2.913	2.093
GOF on F^2	1.049	1.017
R_1[a][$I > 2\sigma(I)$]	0.0296	0.0462
wR_2[b][$I > 2\sigma(I)$]	0.0649	0.0980
R_{int}	0.0273	0.0355
	3	**4**
formula	$C_{30}H_{32}Ag_3Mo_8N_{16}O_{29.5}$	$C_{15}H_{13.5}Ag_2Mo_4N_8O_{14.75}$
fw	2179.85	1141.34
cryst syst	monoclinic	monoclinic
space group	*C*2*m*	*P*2$_1$/*n*
a (Å)	19.278(5)	12.080(5)
b (Å)	25.321(5)	18.297(5)
c (Å)	11.665(5)	12.700(5)
α (°)	90	90
β (°)	104.744(5)	98.770(5)
γ (°)	90	90
V (Å^3)	5507(3)	2774.2(18)
Z	4	4
D_c (g/cm^{-3})	2.629	2.733
GOF on F^2	1.022	1.142
R_1[a][$I > 2\sigma(I)$]	0.0294	0.0361
wR_2[b][$I > 2\sigma(I)$]	0.0606	0.0811
R_{int}	0.0304	0.0256
	5	**6**
formula	$C_{30}H_{25}Ag_2Mo_4N_{16}O_{13.5}$	$C_{15}H_{13}AgMo_4N_8O_{13}$
fw	1425.16	1004.96
cryst syst	triclinic	triclinic
space group	*P*-1	*P*-1
a (Å)	13.029(5)	10.385(5)
b (Å)	13.059(5)	10.488(5)
c (Å)	13.811(5)	12.150(5)
α (°)	71.638(5)	98.289(5)
β (°)	75.025(5)	94.162(5)
γ (°)	63.005(5)	107.191(5)
V (Å^3)	1968.7(13)	1241.7(10)
Z	2	2
D_c (g/cm^{-3})	2.404	2.688
GOF on F^2	1.011	1.020
R_1[a][$I > 2\sigma(I)$]	0.0413	0.0284
wR_2[b][$I > 2\sigma(I)$]	0.0740	0.0579
R_{int}	0.0327	0.0232

[a] $R_1 = \Sigma||F_o| - |F_c||/\Sigma|F_o|$. [b] $wR_2 = |\Sigma w(|F_o|^2 - |F_c|^2)|/\Sigma|w(F_o^2)^2|^{1/2}$.

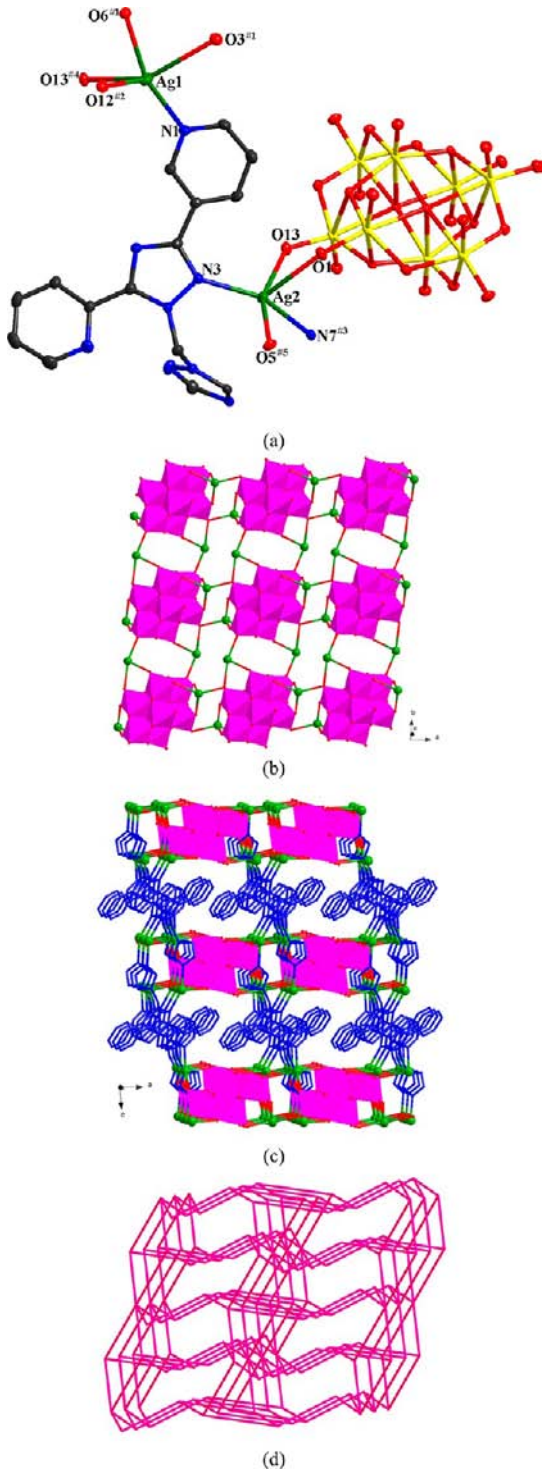

Figure 1. (a) ORTEP view of **1** showing the local coordination environments of Ag(I) ions with hydrogen atoms omitted for clarity (30% probability displacement ellipsoids). Symmetry codes: #1 $-x, -y, -z$; #2 $x, y, z-1$; #3 $-x+1, -y-1, -z+1$; #4 $1-x, -y, -z$; #5 $-x, -1-y, 1-z$. (b) View of the 2D layer formed by the Ag(I) ions and the $[\beta\text{-}Mo_8O_{26}]^{4-}$ anions. (c) View of the 3D framework of **1**. (d) Schematic view of the 3D (3,4,8)-connected framework of **1** with $(4\cdot8^2)(4^2\cdot8^4)(4^3\cdot8^{20}\cdot10^5)$ topology.

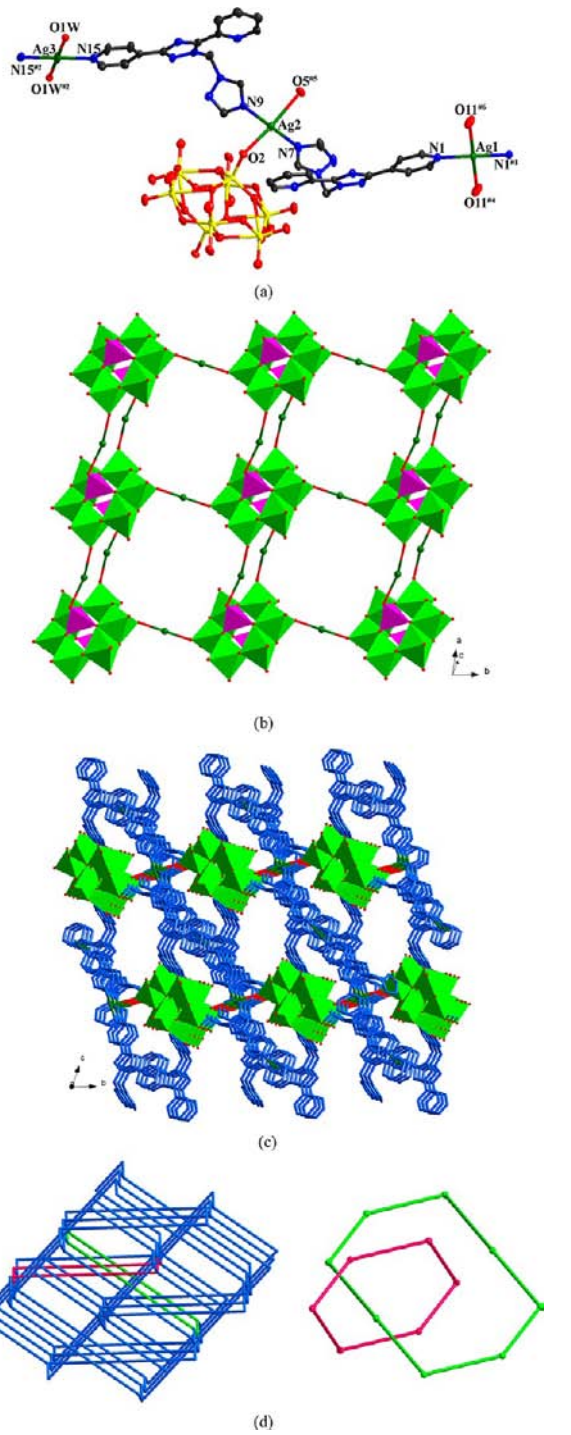

Figure 2. (a) ORTEP view of **2** showing the local coordination environments of Ag(I) ions with hydrogen atoms and lattice water molecules omitted for clarity (30% probability displacement ellipsoids). Symmetry codes: #1 $-x+2, -y+2, -z-2$; #2 $-x, -y-1, -z+1$; #4 $-x+1, -y+2, -z-1$; #5 $x+1, y, z$; #6 $x+1, y, z-1$. (b) View of the 2D layer furnished by Ag1, Ag2 and the $[\beta\text{-}Mo_8O_{26}]^{4-}$ anions. (c) View of the 3D framework of **2**. (d) Schematic view of the 3D (4,6)-connected self-catenated framework with $(6^4\cdot8^2)(4^2\cdot6^3\cdot8^2)$-$(4^2\cdot6^8\cdot8^4\cdot10)$ topology.

molecules. Ag2 is four-coordinated in a tetrahedral coordination geometry, defined by two nitrogen atoms from two different 2,4′-tmbpt ligands and two terminal oxygen atoms from two individual $[\alpha\text{-}Mo_8O_{26}]^{4-}$ anions. The Ag–N bond distances vary from 2.178(5) to 2.198(6) Å and the Ag–O bond lengths range from 2.640(2) to 2.844(5) Å. In **2**, each $[\alpha\text{-}Mo_8O_{26}]^{4-}$ anion coordinates to two Ag1 and four Ag2 ions to yield a 2D layer (part b of Figure 2), which is further linked by

dx.doi.org/10.1021/ic300134z | *Inorg. Chem.* 2012, 51, 11266–11278

the Ag3 ions and the 2,4′-tmbpt ligands to form a 3D framework (part c of Figure 2).

Topologically, if the $[\alpha\text{-}Mo_8O_{26}]^{4-}$ anions can be considered as 6-connected nodes, the Ag1 and Ag2 ions can be viewed as 4-connected nodes, and the Ag3 ions and the 2,4′-tmbpt ligands can be reduced to linkers, the 3D framework of **2** can be simplified as a (4,6)-connected net with $(6^4\cdot8^2)(4^2\cdot6^3\cdot8^2)$-$(4^2\cdot6^8\cdot8^4\cdot10)$ topology. Notably, this net displays a self-catenated pattern, within which the shortest 6-membered rings are catenated by the 8-membered rings belonging to the same framework. Self-catenated structures represent one subclass of the most fascinating topological nets in the family of entanglements, defining as one of the shortest rings being catenated by other shortest rings of the same net.[15] Although families of self-catenated networks have been gradually recognized and designed, the reported examples of self-catenated networks are relatively rare due to the difficulty in controlling the packing geometry of molecules in crystallization.[16,17] A similar known example of 3D self-catenated framework based on octamolybdate is the complex $[Zn(BIMB)_2(\gamma\text{-}Mo_8O_{26})_{0.5}]$ (BIMB = 1,4-bis(1-imidazolyl)-benzene), in which the 6-membered rings are catenated by the 4-membered rings from another inclined layer belonging to the same framework.[18]

Structure of $[Ag_3(3,3'\text{-tmbpt})_2(\alpha\text{-}H_2Mo_8O_{26})_{0.5}(\beta\text{-}Mo_8O_{26})_{0.5}]\cdot3.5H_2O$ (3). The asymmetric unit of **3** consists of one and a half Ag(I) ions, one 3,3′-tmbpt ligand, one-quarter of $[\alpha\text{-}H_2Mo_8O_{26}]^{2-}$ anion, one-quarter of $[\beta\text{-}Mo_8O_{26}]^{4-}$ anion, and one and three-quarters of water molecules. The protonation of the $\alpha\text{-}Mo_8O_{26}$ isomer was determined by the bond valence calculation. The bond valence sum (BVS) value of O14 of the $\alpha\text{-}Mo_8O_{26}$ isomer is 0.95 suggesting that this oxygen atom is monoprotonated (OH).[10b] As shown in part a of Figure 3, Ag1 is five-coordinated in a trigonal biyramid coordination geometry, completed by three nitrogen atoms from three 3,3′-tmbpt ligands and two terminal oxygen atoms from one $[\alpha\text{-}H_2Mo_8O_{26}]^{2-}$ and one $[\beta\text{-}Mo_8O_{26}]^{4-}$ anions. Ag2 is four coordinated in a tetrahedral coordination geometry, defined by two nitrogen atoms from two distinct 3,3′-tmbpt ligands and two terminal oxygen atoms from one $[\alpha\text{-}H_2Mo_8O_{26}]^{2-}$ and one $[\beta\text{-}Mo_8O_{26}]^{4-}$ anions. The Ag–N bond lengths are in the range of 2.181(4)-2.318(4) Å, and the Ag–O bond lengths range from 2.543(3) to 2.859(4) Å. In **3**, each 3,3′-tmbpt as a tetradentate ligand linked the Ag(I) ions to form 1D chains containing large channels with the dimension of about 12.37 × 10.72 Å^2. The $[\beta\text{-}Mo_8O_{26}]^{4-}$ anions, which are located in the channels, link six Ag(I) ions in hexadentate mode (part b of Figure 3). The chains are further connected by the $[\alpha\text{-}H_2Mo_8O_{26}]^{2-}$ anions to form a 3D framework (part c of Figure 3).

From a topological point of view, the $[\alpha\text{-}H_2Mo_8O_{26}]^{2-}$ and $[\beta\text{-}Mo_8O_{26}]^{4-}$ anions can be viewed as two kinds of 6-connected nodes, the 3,3′-tmbpt ligands and the Ag2 ions can be considered as 4-connected nodes, and the Ag1 ions can be reduced to 5-connected nodes. Thus, the complicate 3D framework can be simplified as a (4,5,6)-connected net with $(4^2\cdot6\cdot8^3)(4^4\cdot6\cdot8)(4^6\cdot6^4)(4^{10}\cdot6^5)(4^2\cdot8^8\cdot12^5)$ topology (part d of Figure 3).

Notably, compound **3** is a rare 3D framework based on two kinds of $[Mo_8O_{26}]^{4-}$ isomers.[18] We just reported two examples containing two kinds of octamolybdate isomers, $[Ag_8(L^1)_4(\alpha\text{-}Mo_8O_{26})(\beta\text{-}Mo_8O_{26})(H_2O)_3]\cdot H_2O$ and $[Cu^I_{3.1}Cu^{II}_{0.5}(\beta\text{-}Mo_8O_{26})_{0.5}(\zeta\text{-}Mo_7{}^{VI}Mo^{V}O_{26})_{0.5}(L^2)_2(H_{0.8}L^2)_{0.5}]$ (L^1 = 1,1′-

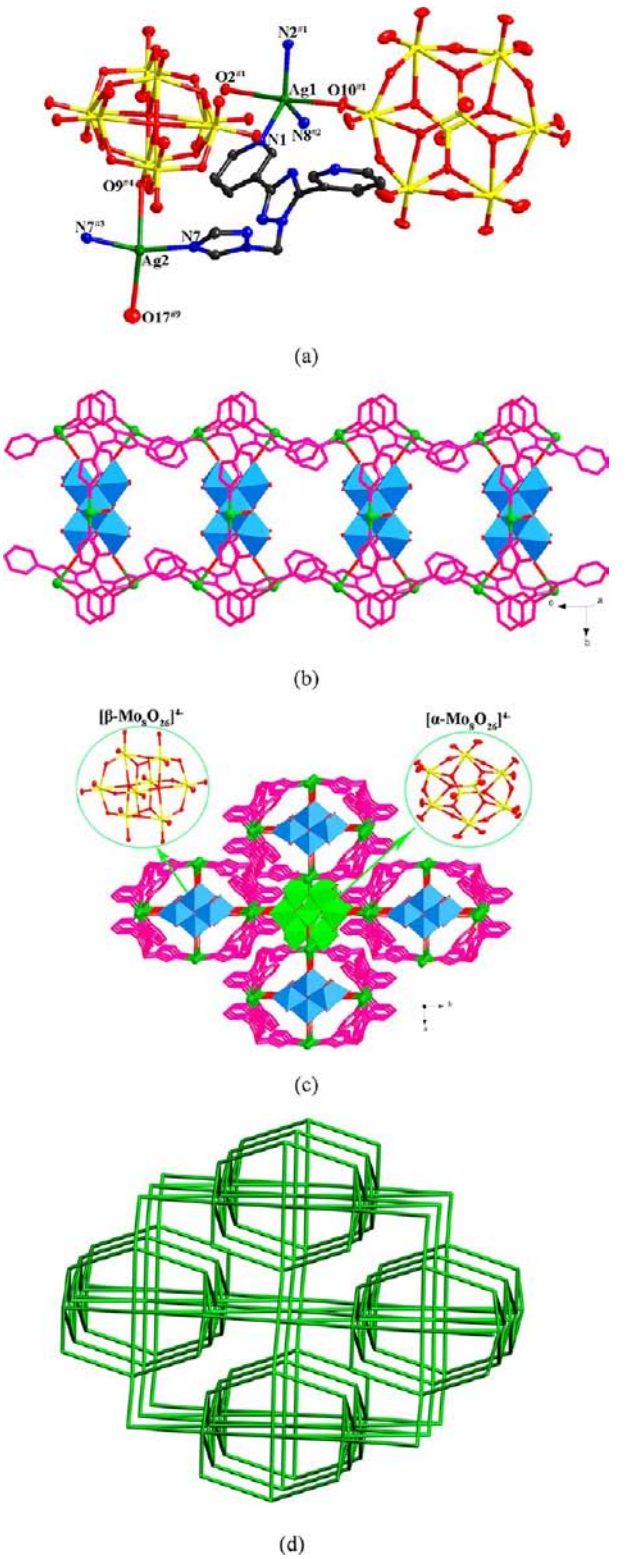

Figure 3. (a) ORTEP view of **3** showing the local coordination environments of Ag(I) ions with hydrogen atoms and lattice water molecules omitted for clarity (30% probability displacement ellipsoids). Symmetry codes: #1 $-x, y, -z+1$; #2 $x, y, z-1$; #3 $x, -y+1, z$; #4 $-x, y, -z+2$; #9 $-1/2+x, 1/2+y, z$. (b) View of the 1D channel occupied by the $[\beta\text{-}Mo_8O_{26}]^{4-}$ anions. (c) Schematic view of the 3D framework of **3**. (d) View of the 3D (4,5,6)-connected framework with $(4^2\cdot6\cdot8^3)(4^4\cdot6\cdot8)(4^6\cdot6^4)(4^{10}\cdot6^5)(4^2\cdot8^8\cdot12^5)$ topology.

dx.doi.org/10.1021/ic300134z | Inorg. Chem. 2012, 51, 11266–11278

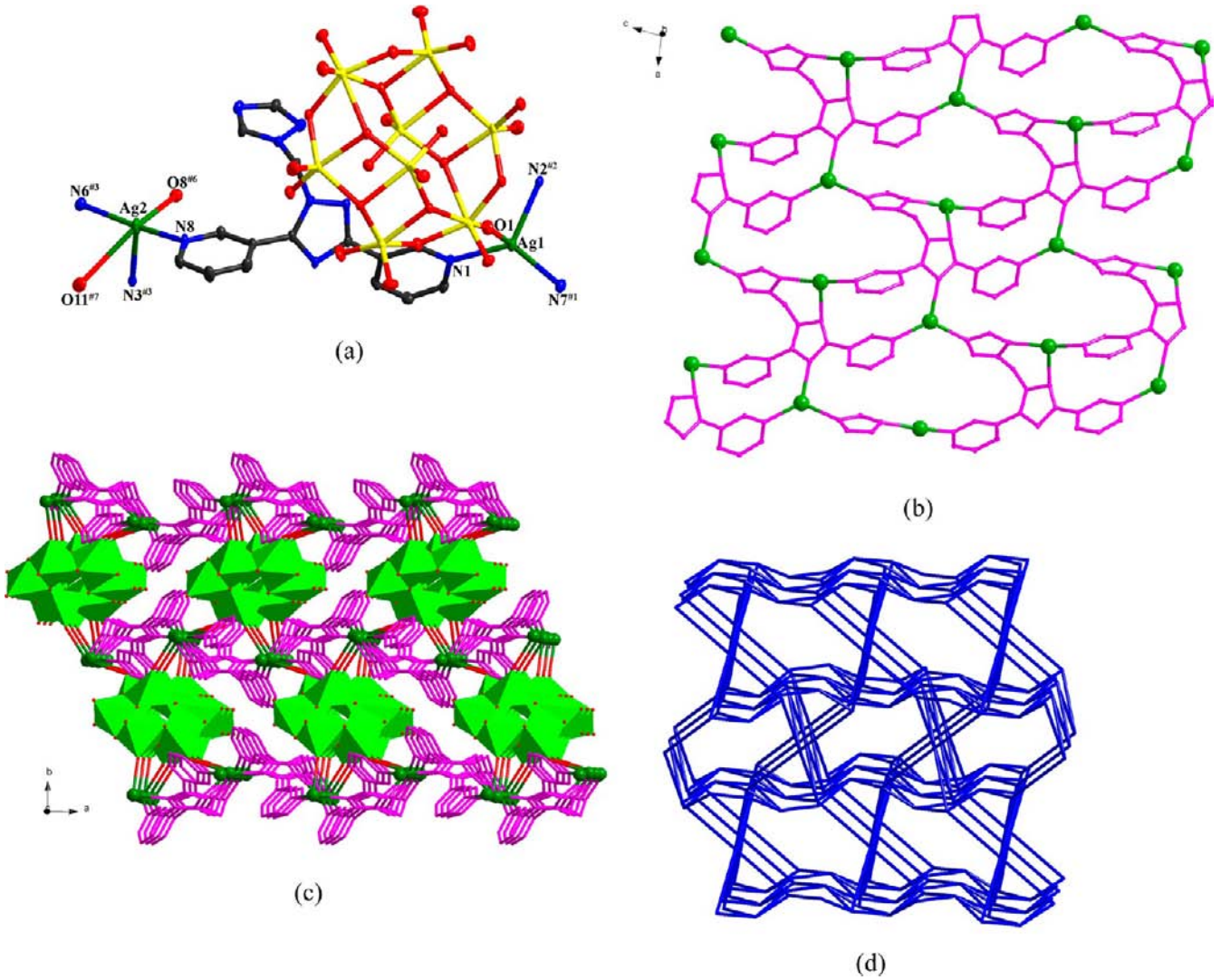

Figure 4. (a) ORTEP view of **4** showing the local coordination environments of Ag(I) ions with hydrogen atoms and lattice water molecules omitted for clarity (30% probability displacement ellipsoids). Symmetry codes: #1 $x, y, z-1$; #2 $x-{}^1/_2, -y-{}^1/_2, z-{}^1/_2$; #3 $x+{}^1/_2, -y-{}^1/_2, z+{}^1/_2$; #6 ${}^3/_2-x, -{}^1/_2+y, {}^3/_2-z$; #7 $2-x, -y, 2-z$. (b) View of 2D Ag-organic fragment of **4**. (c) View of the 3D framework of **4**. (d) Schematic view of the (4,5,6)-connected net with $(4^4{\cdot}6^2)(4^3{\cdot}6^2{\cdot}8)(4^4{\cdot}6^4{\cdot}8^2)(4^2{\cdot}6^7{\cdot}8^4{\cdot}10^2)$ topology.

(1,3-propanediyl)-bis[2-(4-pyridyl)benzimidazole] and L^2 = 1,1′-(1,4-butanediyl)bis[2-(3-pyridyl)benzimidazole]).[19] It should be pointed out that, although a number of hybrid materials containing various octamolybdate isomers have been prepared, examples with two kinds of coexisting octamolybdate clusters in the same crystal are exceedingly rare.[19]

Structure of $[Ag_2(3,3'\text{-tmbpt})(\varepsilon\text{-}Mo_8O_{26})_{0.5}]\cdot 1.75H_2O$ (4). The asymmetric unit of **4** contains two Ag(I) ions, one 3,3′-tmbpt ligand, half a $[\varepsilon\text{-}Mo_8O_{26}]^{4-}$ anion, and one and three-quarters of water molecules. Each $[\varepsilon\text{-}Mo_8O_{26}]^{4-}$ anion consists of six $\{MoO_5\}$ square pyramids and two $\{MoO_6\}$ octahedra linked by edge-sharing interactions into an ellipsoidal cluster.[20] As shown in part a of Figure 4, Ag1 is four-coordinated by one oxygen atom from one $[\varepsilon\text{-}Mo_8O_{26}]^{4-}$ anion and three nitrogen atoms from three distinct 3,3′-tmbpt ligands in a tetrahedral coordination geometry. Ag2 is five-coordinated by two oxygen atoms from two individual $[\varepsilon\text{-}Mo_8O_{26}]$ anions and three nitrogen atoms from two different 3,3′-tmbpt ligands in a trigonal biyramid coordination geometry. The Ag−N bond lengths range from 2.182(5) to 2.545(5) Å, and the Ag−O bond lengths change from 2.594(6) to 2.865(5) Å. In **4**, each 3,3′-tmbpt ligand links five Ag(I) ions to form a 2D sheet (part b of Figure 4), which is further extended by the $[\varepsilon\text{-}Mo_8O_{26}]^{4-}$ anions to furnish a 3D framework (part c of Figure 4).

Topologically, if the $[\varepsilon\text{-}Mo_8O_{26}]^{4-}$ anions can be reduced to 6-connected nodes, the 3,3′-tmbpt ligands can be viewed as 5-connected nodes and the Ag(I) ions can be considered as 4-connected nodes, the 3D framework can be simplified as a (4,5,6)-connected net with $(4^4{\cdot}6^2)(4^3{\cdot}6^2{\cdot}8)(4^4{\cdot}6^4{\cdot}8^2)$-$(4^2{\cdot}6^7{\cdot}8^4{\cdot}10^2)$ topology (part d of Figure 4).

Up to now, a number of hybrid materials containing various octamolybdate isomers have been prepared. However, the ones based on $[\varepsilon\text{-}Mo_8O_{26}]^{4-}$ isomers are particularly rare.[20]

Structure of $[Ag_2(3,4'\text{-tmbpt})_2(\beta\text{-}Mo_8O_{26})_{0.5}]\cdot 0.5H_2O$ (5). The asymmetric unit of **5** contains two Ag(I) ions, two 3,4′-tmbpt ligands, half a $[\beta\text{-}Mo_8O_{26}]^{4-}$ anion and half a water molecule. As shown in part a of Figure 5, Ag1 is four-coordinated by three nitrogen atoms from three individual 3,4′-tmbpt ligands and one oxygen atom from one $[\beta\text{-}Mo_8O_{26}]^{4-}$ anion in a tetrahedral coordination geometry. Ag2 is two-coordinated by two nitrogen atoms from two distinct 3,4′-tmbpt ligands showing an approximately linear coordination

dx.doi.org/10.1021/ic300134z | Inorg. Chem. 2012, 51, 11266−11278

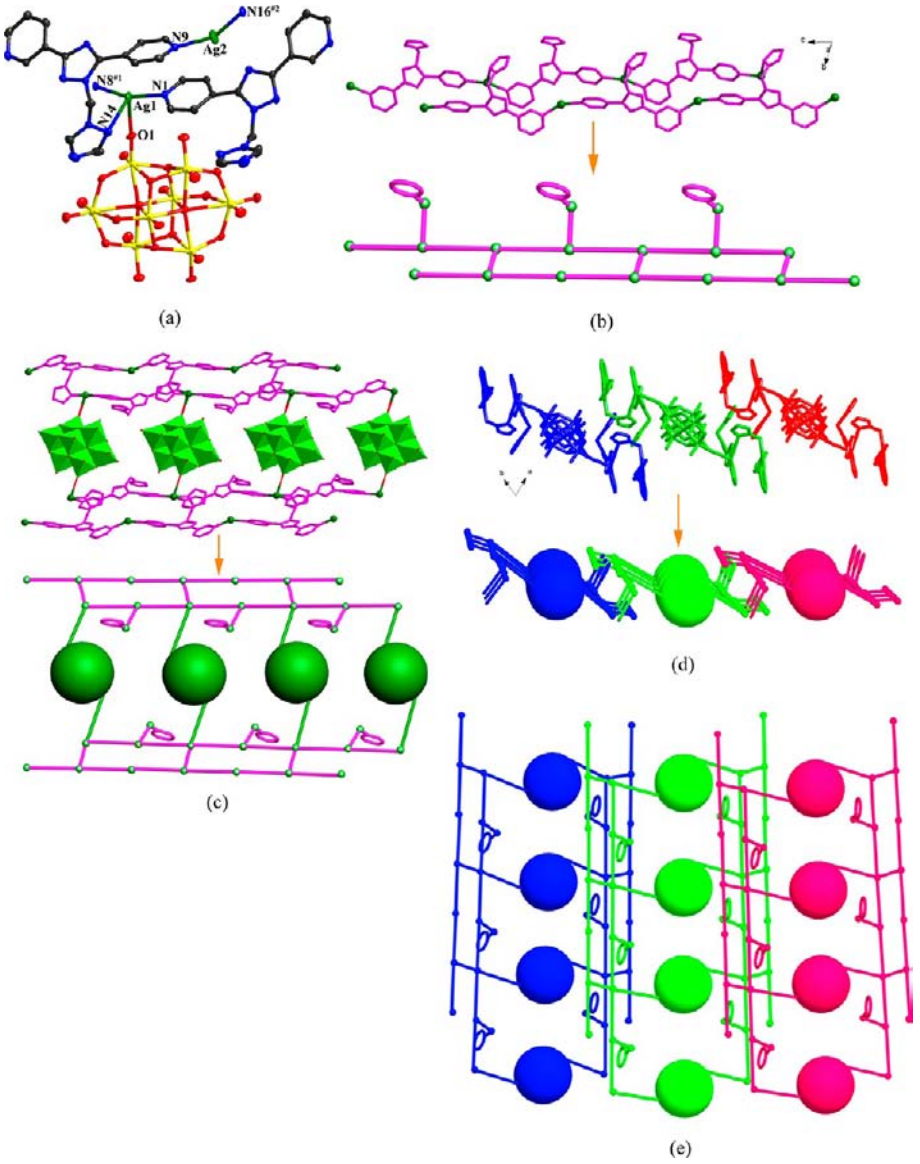

Figure 5. (a) ORTEP view of **5** showing the local coordination environments of Ag(I) ions with hydrogen atoms and lattice water molecules omitted for clarity (30% probability displacement ellipsoids). Symmetry codes: $^{\#1}$ $x, y, z - 1$; $^{\#2}$ $x, y, z + 1$. (b) View of the 1D chain formed by Ag(I) ions and the 3,4-tmbpt ligands. (c) View of the 1D chain of **5**. (d) Side view of the 1D → 2D polythreaded structure of **5**. (e) Front view of the 1D → 2D polythreaded structure of **5**.

environment. The Ag−N bond lengths are in the range of 2.139(4)−2.817(6) Å and the Ag−O bond distance is 2.583(4) Å. In **5**, two kinds of 3,4′-tmbpt ligands show bidentate and tridentate coordination modes. The two kinds of the 3,4′-tmbpt ligands linked the Ag(I) ions to form a double chain (part b of Figure 5). A pair of the double chains are further connected by the $[\beta\text{-}Mo_8O_{26}]^{4-}$ anions to form an inorganic−organic hybrid chain (part c of Figure 5).

Better insight into the structure, it can be found that the free triazolyl groups in the bidentate 3,4′-tmbpt ligands act as arms and thread into the windows of the adjacent chains, resulting in a rare 1D → 2D polythreaded structure (parts d and e of Figure 5). Until now, although a number of ploythreaded structures have been reported, the ones based on octamolybdates are exceedingly rare.[2d]

Structure of [Ag(3,4′-Htmbpt)(β-Mo_8O_{26})$_{0.5}$] (6). The asymmetric unit of **6** contains one Ag(I) ion, one protonated 3,4′-tmbpt ligand (3,4′-Htmbpt) and half a $[\beta\text{-}Mo_8O_{26}]^{4-}$ anion. As shown in part a of Figure 6, Ag1 is five-coordinated in a trigonal biyramid coordination geometry, furnished by two nitrogen atoms from two different 3,4′-Htmbpt ligands (Ag(1)−N(1) = 2.203(4) and Ag(1)−N(7)$^{\#1}$ = 2.218(4) Å) and three terminal oxygen atoms from two distinct $[\beta\text{-}Mo_8O_{26}]^{4-}$ anions (Ag(1)−O(8)$^{\#2}$ = 2.577(3), Ag(1)−O(6)$^{\#2}$ = 2.651(3), and Ag(1)−O(8)$^{\#7}$ = 2.666(3) Å). Each 3,4′-Htmbpt ligand links two Ag(I) ions to form a infinite chain (part b of Figure 6), which is further extended by the $[\beta\text{-}Mo_8O_{26}]^{4-}$ anions to form a 2D layer (part c of Figure 6). Moreover, there are intermolecular N−H···O hydrogen bonding interactions between N8 of the 3,4′-Htmbpt ligands and O5 of the $[\beta\text{-}Mo_8O_{26}]^{4-}$ anions (d(N8···O5) = 2.726(6) Å and ∠N8−H8A···O5 = 149.3°), which further linked the layers into a 3D supramolecular architecture (part d of Figure 6).

Structural Patterns and Coordination Modes of $[Mo_8O_{26}]^{4-}$ Anions. Usually, the $[Mo_8O_{26}]^{4-}$ anions can display several kinds of structural patterns and coordinate to

dx.doi.org/10.1021/ic300134z | *Inorg. Chem.* 2012, 51, 11266−11278

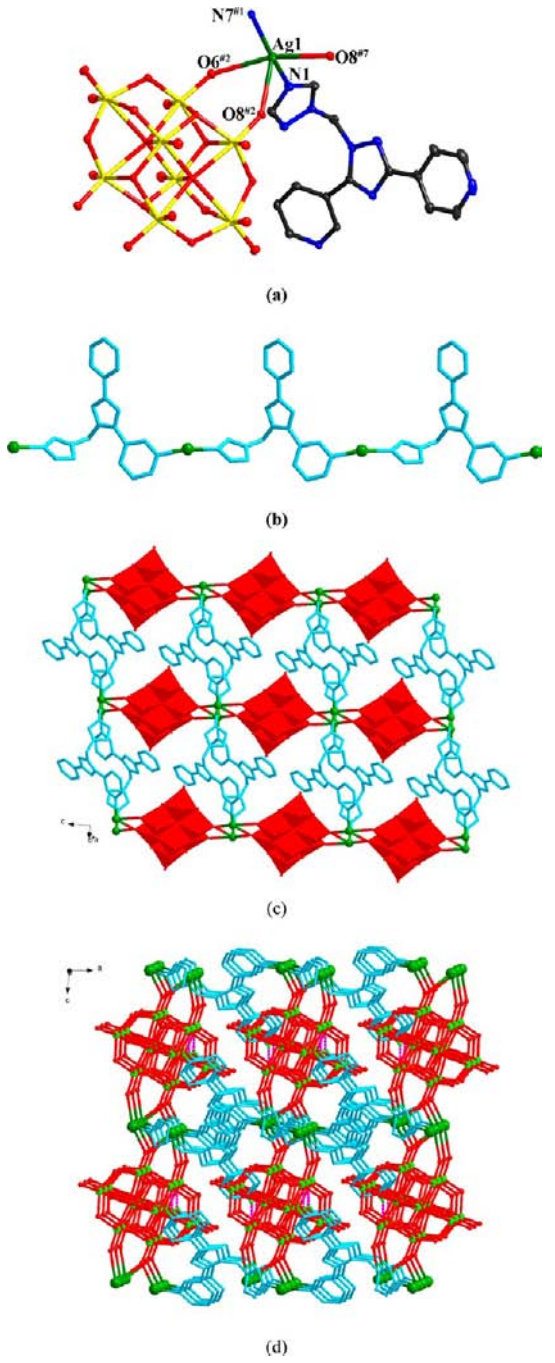

Figure 6. (a) ORTEP view of **6** showing the local coordination environment of Ag(I) ion with hydrogen atoms omitted for clarity (30% probability displacement ellipsoids). Symmetry codes: #1 $x-1, y-1, z$; #2 $x-1, y-1, z-1$; #7 $-x, -y, 2-z$. (b) View of the 1D chain formed by Ag(I) ions and the 3,4′-tmbpt ligands. (c) View of the 2D sheet of **6**. (d) Schematic view of 3D supramolecular architecture of **6**.

metal ions in a variety of coordination modes to form attractive compounds with different structures.[3−5] In compounds **1**−**6**, the $[Mo_8O_{26}]^{4-}$ anions exhibit three kinds of structural forms (α, β and ε) and seven types of coordination modes (Scheme 2). The β-$[Mo_8O_{26}]^{4-}$ anions in compounds **1**, **3**, **5**, and **6** act as octadentate, hexadentate, bidentate, and tetradentate ligands coordinating to eight, six, two, and four Ag(I) ions, respectively. As far as we know, the coordination mode of the β-$[Mo_8O_{26}]^{4-}$ anion in **1** are rarely observed in inorganic−organic hybrid materials. The α-$[Mo_8O_{26}]^{4-}$ and α-$[H_2Mo_8O_{26}]^{2-}$ anions in compounds **2** and **3** act as hexadentate ligands, but their coordination modes are different. In **2**, the oxygen atoms coordinated to the Ag(I) ions are from six different molybdenum atoms, while, in **3**, the correspongding ones are from four different molybdenum atoms. The ε-$[Mo_8O_{26}]^{4-}$ anions in compound **4** act as hexadentate ligands, coordinating to six Ag(I) ions through its terminal oxygen atoms. Clearly, the structural patterns and the coordination modes of octamolybdate anions have important effects on the inorganic−organic hybrid materials.

Moreover, the tmbpt ligands exhibited a variety of coordination modes through bridging two, three, four, and five Ag(I) ions (Scheme 3), which further influenced the final structures of the compounds.

Effect of pH Value on Framework. It is well established that pH values can influence the protonated extents of the organic ligands.[5,21] Take compounds **5** and **6** for example. When the pH value was 2, one N atom of the pyridine rings from the 3,4′-tmbpt ligand is protonated restricting itself to coordinate to Ag(I) ion in **6**. Thus, the 3,4′-tmbpt ligand linked the Ag(I) to form a 1D chain in a bidentate mode, which is extended by the $[\beta$-$Mo_8O_{26}]^{4-}$ anions into a 2D layer. When the pH value is adjusted to 3, compound **5** is obtained. In **5**, all the nitrogen atoms are nonprotonated. The 3,4′-tmbpt ligands linked the Ag(I) ions to form a double chain. A pair of the chains are connected by the $[\beta$-$Mo_8O_{26}]^{4-}$ anions to form an inorganic−organic hybrid chain. The free triazolyl groups as arms thread into the windows of the adjacent chains, resulting in an interesting 1D → 2D polythreaded structure.

Stabilization of Mo_8O_{26} Isomers. It is well-known that several factors, such as reaction temperatures,[22a] countercations,[22b] hydrogen-bonding interactions[22a,c] and metal−organic motifs,[23] can influence the stabilization of the different Mo_8O_{26} isomers. For compounds $[Ag_3(3,3'\text{-tmbpt})_2(\alpha\text{-}H_2Mo_8O_{26})_{0.5}(\beta\text{-}Mo_8O_{26})_{0.5}]\cdot 3.5H_2O$ (**3**) and $[Ag_2(3,3'\text{-tmbpt})(\varepsilon\text{-}Mo_8O_{26})_{0.5}]\cdot 1.75H_2O$ (**4**), the Ag(I)-tmbpt motifs and the hydrogen-bonding interactions involved in Mo_8O_{26} isomers are the two main possible factors that influence the stabilization of the Mo_8O_{26} isomers. Compared with the $[\varepsilon$-$Mo_8O_{26}]^{4-}$ anion in **4**, each $[\alpha$-$H_2Mo_8O_{26}]^{2-}$ anion in **3** has two additional H atoms on the O atoms. Therefore, the protonated O atoms in **3** can serve as H donors to participate in the formation of hydrogen-bonding interactions. However, in **4**, the O atoms of the $[\varepsilon$-$Mo_8O_{26}]^{4-}$ anions can only act as H acceptors. In addition, the different Ag(I)-tmbpt motifs between **3** and **4** is another possible factor that influences the stabilization of the Mo_8O_{26} isomers.[23] The Ag(I)-tmbpt motif in **3** shows a 1D tubelike chain structure, whereas it displays a 2D layer structure in **4**. Further, in **3**, the $[\beta$-$Mo_8O_{26}]^{4-}$ anions are located in the channels of the tubelike chains, while the $[\alpha$-$H_2Mo_8O_{26}]^{2-}$ anions bridge the tubelike chains as linkers. In **4**, each $[\varepsilon$-$Mo_8O_{26}]^{4-}$ anion only interacts with two adjacent layers through the Ag−O bonds.

Optical Band Gaps. To investigate the conductivity potentials of compounds **1**−**6**, the diffuse reflectivity for powder samples of **1**−**6** were performed to obtain the band gap (E_g). The absorption (α/S) data were calculated from the reflectivity using the Kubelka−Munk function: $\alpha/S = (1-R)^2/2R$ where R is the reflectivity at a given wavelength, α is the absorption coefficient, and S is the scattering coefficient.[22b] The band gap was determined as the intersection point between the energy axis at $\alpha/S = 0$ and the line extrapolated from the linear

dx.doi.org/10.1021/ic300134z | Inorg. Chem. 2012, 51, 11266−11278

Scheme 2. Coordination Modes of $[Mo_8O_{26}]^{4-}$ Anions

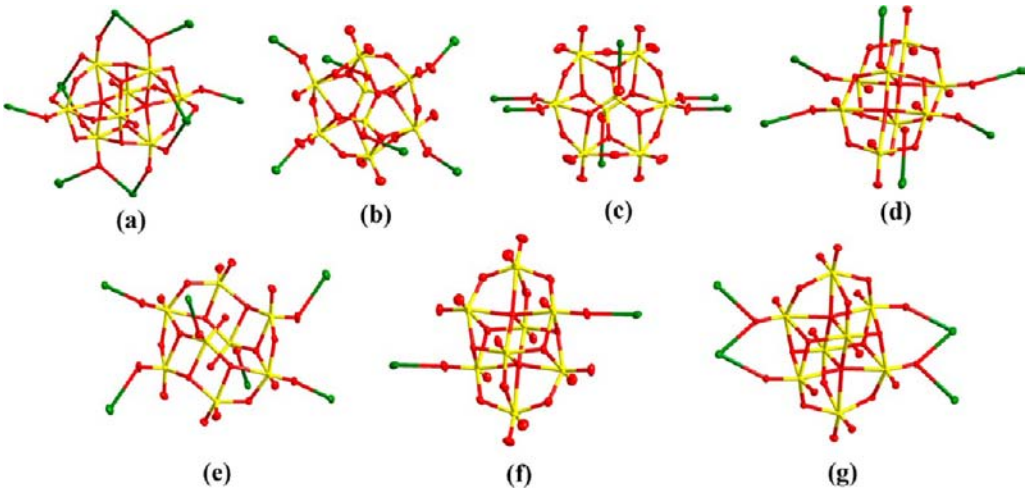

Scheme 3. Coordination Modes of the tmbpt Ligands

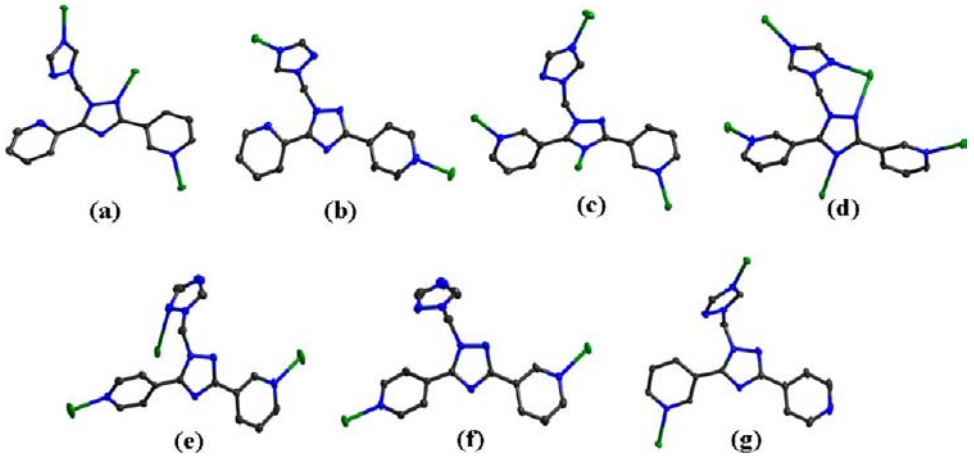

portion of the adsorption edge in a plot of α/S against energy E.[22b] The α/S versus E plots are shown in Figure 7. For compounds **1**–**6**, the well-defined optical absorption associated with band gaps (E_g) can be assessed at 3.23, 2.88, 2.94, 2.96, 2.78, and 3.39 eV, respectively. The reflectance spectra imply that compounds **1**–**6** are potential semiconductors with wide band gaps.[18] In addition, the optical band gaps have been measured for the tmbpt ligands. The E_g values of the 2,3′-tmbpt, 2,4′-tmbpt, 3,3′-tmbpt and 3,4′-tmbpt ligands are 3.69, 3.87, 3.73, and 3.73 eV, respectively (Figure S2 of the Supporting Information), which are much higher than those of **1**–**6**. Therefore, the optical band gaps of **1**–**6** are not relevant to the tmbpt ligands. The optical band gaps can be assigned to $[Ag^I_4(Mo_8O_{26})]_n$ for **1**, **2**, **4**, and **5**, $\{[Ag^I_6(\alpha\text{-}H_2Mo_8O_{26})(\beta\text{-}Mo_8O_{26})]^{2-}\}_n$ for **3** and $\{[Ag^I_2(Mo_8O_{26})]^{2-}\}_n$ for **6**, respectively.[24]

Photoluminescent Properties. The photoluminescent properties of the tmbpt ligands and compounds **1**–**6** have been studied in the solid state at room temperature. The emission and excitation peaks of the tmbpt ligands are shown in Figure S3 of the Supporting Information and the emission peaks of compounds **1**–**6** are shown in Figure 8.

The 2,3′-tmbpt, 2,4′-tmbpt, 3,3′-tmbpt and 3,4′-tmbpt show emission peaks at 526 nm (λ_{ex} = 438 nm), 560 nm (λ_{ex} = 434 nm), 441 (λ_{ex} = 344 nm) and 554 nm (λ_{ex} = 328 nm), respectively. These emissions may be attributed to the π^*-n or $\pi^*-\pi$ transition.[25] Upon complexation of these ligands with Ag(I) ions and the $[Mo_8O_{26}]^{4-}$ anions, the emission peaks occur at 457 nm (λ_{ex} = 423 nm) for **1**, 462 nm (λ_{ex} = 423 nm) for **2**, 471 nm (λ_{ex} = 423 nm) for **3**, 447 nm (λ_{ex} = 412 nm) for **4**, 439 nm (λ_{ex} = 408 nm) for **5**, and 438 nm (λ_{ex} = 408 nm) for **6**, respectively. The emission peaks of compounds **3** and **4** are similar to that of the free 3,3′-tmbpt ligand, so the emissions of these compounds can probably be attributed to the intraligand fluorescent emissions.[26] However, for compounds **1**, **2**, **5**, and **6**, the emission peaks are highly blue-shifted compared to the free tmbpt ligands. This may be attributed to the coordination effects of the tmbpt ligands to Ag(I) ions, which increase the conformation rigidity of the ligands and reduce the nonradiative decay of the intraligand.[27]

Photocatalytic Properties. Photocatalytic properties have attracted much interest attributed to their potential applications in purifying water and air by decomposing organic compounds.[28] In this work, methylene blue (MB), which is typically difficult to decompose in wastewater,[29] was selected for evaluating the activity of photocatalysts toward the decomposition of organic pollutants. We have studied the photocatalytic behaviors of compounds **3**–**6** for the photodegradation of MB under UV irradiation. The results indicate that compounds **3**–**6** have good catalytic effectiveness. As

dx.doi.org/10.1021/ic300134z | Inorg. Chem. 2012, 51, 11266–11278

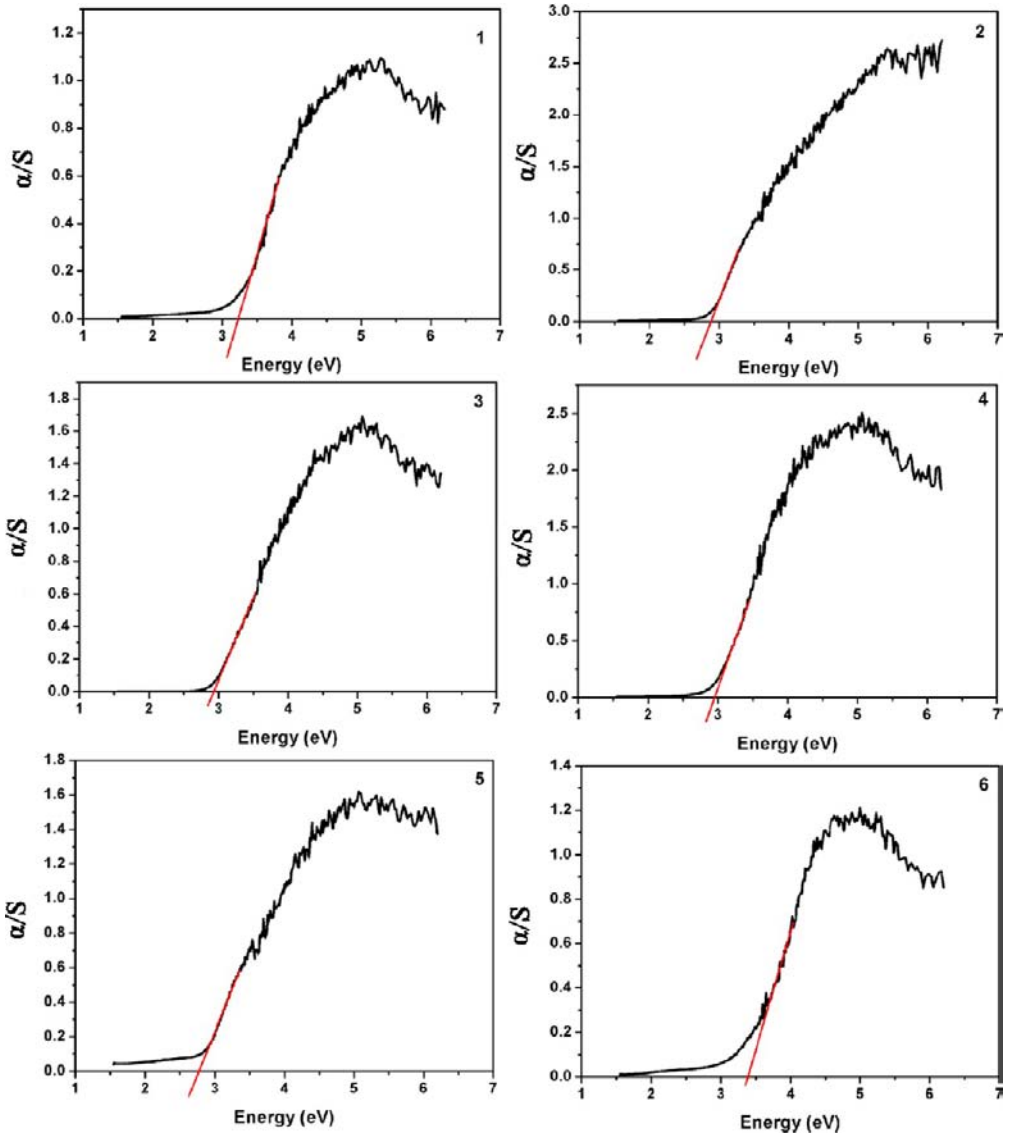

Figure 7. UV−vis-NIR diffuse reflectance spectra of K−M functions vs energy (eV) of compounds **1**−**6**.

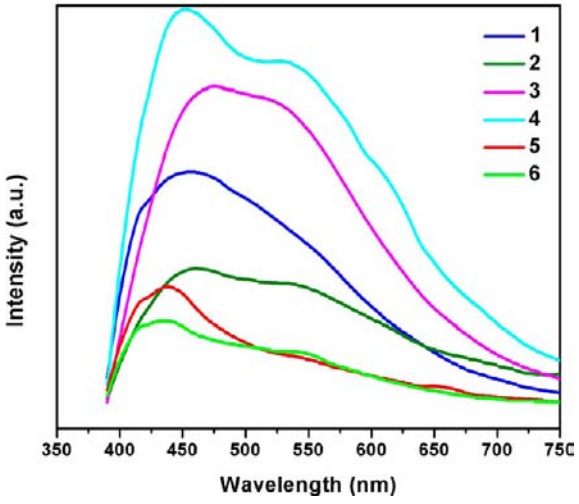

Figure 8. Solid-state photoluminescent emission spectra of compounds **1**−**6** at room temperature.

shown in Figure 9, the absorption peaks of MB decreased obviously. In addition, the concentrations of MB (C) against reaction times (t) of compounds **3**−**6** are shown in Figure10. It can be seen that the photocatalytic activities increase from 24% (without any catalyst) to 80% for **3**, 91% for **4**, 84% for **5**, and 91% for **6** after 1.5 h of irradiation. These results suggest that compounds **3**−**6** are good candidates for photocatalytic degradation of MB.

In addition, the specific surface areas for **3**−**6** have been measured. The BET areas (S_{BET}) for **3**-**6** are 1.38, 1.36, 0.43, and 2.15 m^2/g, respectively. As we expected, these values are very low because of their nonporous structures.[30] Among these four compounds, **6** and **5** have the highest and the lowest S_{BET} values, respectively. This result is almost consistent with regulation that the photocatalytic performances of compounds depend on their specific surface areas to some extent.[31] However, the ones of **3** and **4** do not well correspond to this regulation. This result indicates that the specific surface areas may be not a dominant factor that influences the photocatalytic activities of **3** and **4**.

dx.doi.org/10.1021/ic300134z | *Inorg. Chem.* 2012, 51, 11266−11278

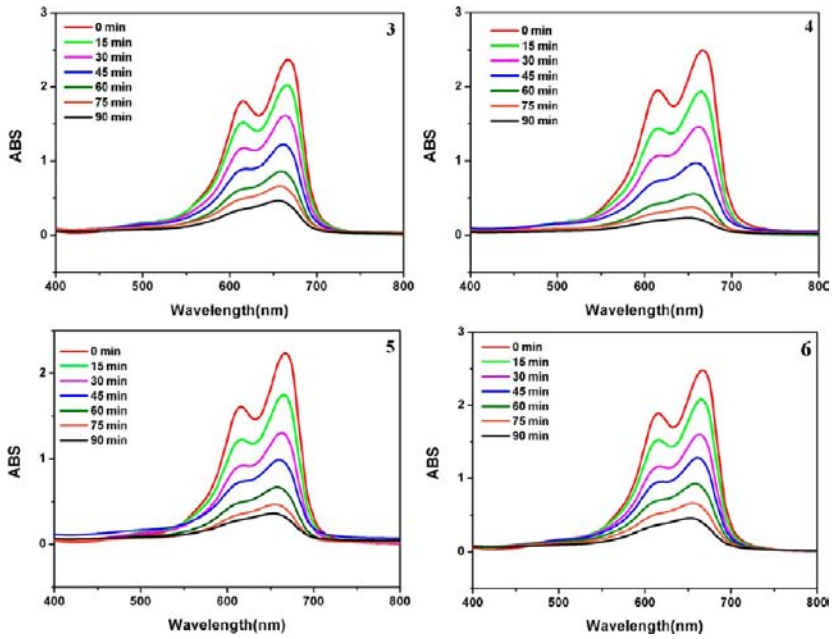

Figure 9. Absorption spectra of the MB solution during the decomposition reaction under UV light irradiation with the use of compounds **3**–**6**.

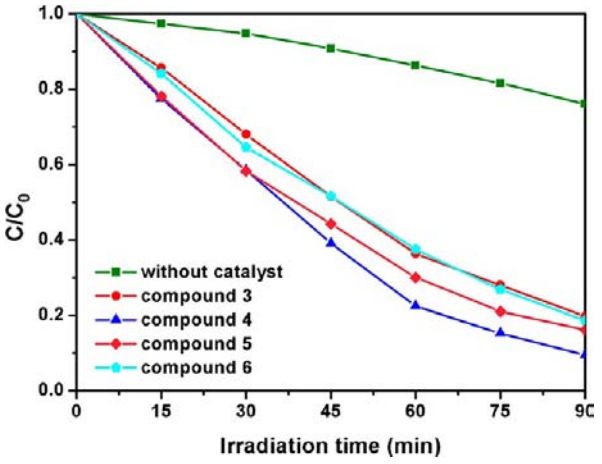

Figure 10. Photocatalytic decomposition of MB solution under UV with the use of compounds **3**–**6** and the control experiment without any catalyst.

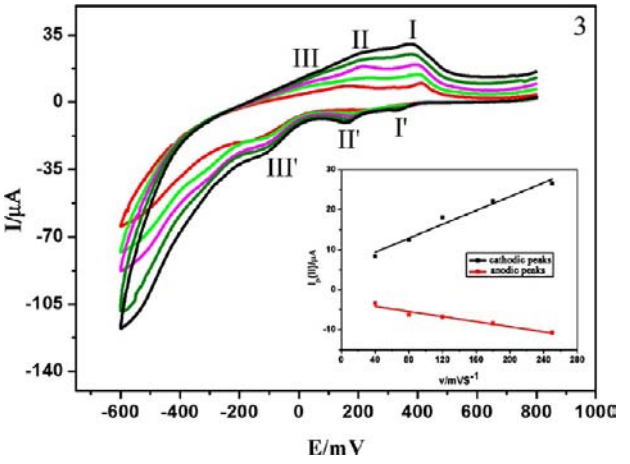

Figure 11. Cyclic voltammograms of 1-CPE in 1 M H_2SO_4 at different scan rates (from inner to outer: 40, 80, 120, 180, 250 mV s^{-1}). The insert shows plots of the anodic and the cathodic peak currents of II–II′ against scan rates.

Cyclic Voltammetry. Compound **3** has been taken as an example to study electrochemical property. The electrochemical behaviors of **3**-modified carbon paste electrode (**3**-CPE) at different scan rates were investigated in 1 mol L^{-1} H_2SO_4 aqueous solution. As shown in Figure 11, three pairs of reversible redox peaks (I–I′, II–II′, III–III′) appeared in the potential range from −600 to 800 mV. The mean peak potentials ($E_{1/2}$ = (E_{pa} + E_{pc})/2) are +348 mV (I), +181 mV (II) and −45 mV (III), respectively (versus Ag/AgCl; scan rate, 100 mV s^{-1}). Redox peaks I–I′, II–II′, and III–III′ can be ascribed to three consecutive two-electron processes.[32] The peak potentials change gradually following the scan rates from 40 to 250 mV s^{-1} for **3**-CPE: the cathodic peak potentials shift toward the negative direction and the corresponding anodic peak potentials to the positive direction with increasing scan rates. The results indicate that the redox ability of the polyanions can be maintained in the hybrid solids.[33] As the scan rate varied from 40 to 250 mV s^{-1}, the peak currents were approximate proportional to the scan rate, which indicates the redox process is surface-controlled.[32a,34]

CONCLUSIONS

In conclusion, series of inorganic–organic hybrid materials based on octamolybdates, Ag(I) ions and multidentate N-donor ligands have been successfully synthesized under hydrothermal conditions. These materials exhibit fascinating 2D and 3D structures with the $[Mo_8O_{26}]^{4-}$ anions in various structural patterns. The results imply that the coordination modes of the octamolybdate anions and the tmbpt ligands as well as the pH values play important roles in the formation of the hybrid materials. The solid-state fluorescence spectra indicate that compounds **1**–**6** have intense photoluminesce at room temperature. The photocatalytic behaviors of compounds **3**–**6** show that they are good candidates for photocatalytic degradation of MB.

dx.doi.org/10.1021/ic300134z | Inorg. Chem. 2012, 51, 11266–11278

■ ASSOCIATED CONTENT

Supporting Information

X-ray crystallographic files (CIF), PXRD patterns, selected bond lengths and angles, and photoluminescent spectra. This material is available free of charge via the Internet at http://pubs.acs.org.

■ AUTHOR INFORMATION

Corresponding Author

*E-mail: yangjinnenu@yahoo.com.cn (J.Y.); jianfangma@yahoo.com.cn, fax: +86-431-85098620 (J.-F.M.).

Notes

The authors declare no competing financial interest.

■ ACKNOWLEDGMENTS

We thank the National Science Foundation of China (21001023 and 21071028), the Specialized Research Fund for the Doctoral Program of Higher Education, the Science Foundation of Jilin Province (201215005 and 20100109), and the Fundamental Research Funds for the Central Universities for support.

■ REFERENCES

(1) (a) Kogerler, P.; Cronin, L. *Angew. Chem., Int. Ed.* **2005**, *44*, 844. (b) Yamase, T. *Chem. Rev.* **1998**, *98*, 307. (c) Dolbecq, A.; Dumas, E.; Mayer, C. R.; Mialane, P. *Chem. Rev.* **2010**, *110*, 6009. (d) Mizuno, N.; Yamaguchi, K.; Kamata, K. *Coord. Chem. Rev.* **2005**, *249*, 1944. (e) Xu, L.; Lu, M.; Xu, B. B.; Wei, Y. G.; Peng, Z. H.; Powell, D. R. *Angew. Chem., Int. Ed.* **2002**, *41*, 4129. (f) Song, J.; Luo, Z.; Britt, D. K.; Furukawa, H.; Yaghi, O. M.; Hardcastle, K. I.; Hill, C. L. *J. Am. Chem. Soc.* **2011**, *133*, 16839. (g) Coronado, E.; Gómez-García, C. J. *Chem. Rev.* **1998**, *98*, 273. (h) Schemberg, J.; Schneider, K.; Demmer, U.; Warkentin, E.; Müller, A.; Ermler, U. *Angew. Chem., Int. Ed.* **2007**, *119*, 2460. (i) Vasylyev, M. V.; Neumann, R. *J. Am. Chem. Soc.* **2004**, *126*, 884. (j) Wu, H.; Yang, J.; Su, Z.-M.; Batten, S. R.; Ma, J.-F. *J. Am. Chem. Soc.* **2011**, *133*, 11406.

(2) (a) Meng, J. X.; Lu, Y.; Li, Y. G.; Fu, H.; Wang, E. B. *Cryst. Growth Des.* **2009**, *9*, 4116. (b) Meng, X.; Qin, C.; Wang, X.-L.; Su, Z.-M.; Li, B.; Yang, Q.-H. *Dalton Trans.* **2011**, *40*, 9964. (c) Zheng, S.-T.; Yang, G.-Y. *Dalton Trans.* **2010**, *39*, 700. (d) Lan, Y.-Q.; Li, S.-L.; Wang, X.-L.; Shao, K.-Z.; Du, D.-Y.; Zang, H.-Y. *Inorg. Chem.* **2008**, *47*, 8179.

(3) (a) Kong, Z. P.; Weng, L. H.; Tan, D. J.; He, H. Y.; Zhang, B.; Kong, J. L.; Yue, B. *Inorg. Chem.* **2004**, *43*, 5676. (b) Hagrman, D.; Sangregorio, C.; O'Connor, C. J.; Zubieta, J. *J. Chem. Soc., Dalton Trans.* **1998**, 3707. (c) Rarig, R. S.; Zubieta, J. *Polyhedron* **2003**, *22*, 177. (d) Allis, D. G.; Rarig, R. S.; Burkholder, E.; Zubieta, J. *J. Mol. Struct.* **2004**, *688*, 11. (e) Wu, C. D.; Lu, C. Z.; Zhuang, H. H.; Huang, J. S. *Inorg. Chem.* **2002**, *41*, 5636. (f) Zang, H. Y.; Tan, K.; Guan, W.; Li, S.-L.; Yang, G. S.; Shao, K.-Z.; Yan, L.-K.; Su, Z.-M. *CrystEngComm* **2010**, *12*, 3684.

(4) (a) Li, S.-L; Lan, Y.-Q.; Ma, J.-F.; Yang, J.; Wang, X.-H.; Su, Z.-M. *Inorg. Chem.* **2007**, *46*, 8283. (b) Xiao, D. R.; Hou, Y.; Wang, E. B.; Wang, S. T.; Li, Y. G.; Xu, L.; Hu, C. W. *Inorg. Chim. Acta* **2004**, *357*, 2525.

(5) Liu, H. Y.; Wu, H.; Yang, J.; Liu, Y. Y.; Liu, B.; Liu, Y. Y.; Ma, J.-F. *Cryst. Growth Des.* **2011**, *11*, 2920.

(6) (a) Yang, M. X.; Chen, L. J.; Lin, S.; Chen, X. H.; Huang, H. *Dalton Trans.* **2011**, *40*, 1866. (b) An, H. Y.; Li, Y. G.; Wang, E. B.; Xiao, D. R.; Sun, C. Y.; Xu, L. *Inorg. Chem.* **2005**, *44*, 6062. (c) Lin, F. X.; Marchal-Roch, C.; Bouchard, P.; Marrot, J.; Simonato, J. P.; Hervé, G.; Sécheresse, F. *Inorg. Chem.* **2004**, *43*, 2240.

(7) (a) Browne, W. R.; O'Connor, C. M.; Hughes, H. P.; Hage, R.; Walter, O.; Doering, M.; Gallagher, J. F.; Vos, J. G. *J. Chem. Soc., Dalton Trans.* **2002**, 4048. (b) Liu, H. Y.; Wu, H.; Ma, J.-F.; Liu, Y. Y.; Liu, B.; Yang, J. *Cryst. Growth Des.* **2010**, *10*, 4795. (c) Yang, J.; Ma, J.-F.; Liu, Y. Y.; Ma, J. C.; Batten, S. R. *Cryst. Growth Des.* **2008**, *8*, 4383. (d) Zhang, L. P.; Ma, J.-F.; Pang, Y.-Y.; Ma, J.-C.; Yang, J. *CrystEngComm.* **2010**, *12*, 4433.

(8) (a) Sheldrick, G. M. SHELXS-97, *Programs for X-ray Crystal Structure Solution*; University of Göttingen: Göttingen, Germany, 1997. (b) Sheldrick, G. M. SHELXL-97, *Programs for X-ray Crystal Structure Refinement*; University of Göttingen: Göttingen, Germany, 1997.

(9) Cochran, W.; Lipson, H. *The Determination of Crystal Structures*. Ithaca, NY: Cornell University Press, 1966, 323.

(10) (a) Brown, I. D.; Altermatt, D. *Acta Crystallogr.* **1985**, *B41*, 244. (b) Fang, X.; Kögerler, P. *Angew. Chem., Int. Ed.* **2008**, *47*, 8123.

(11) (a) Zhang, C. J.; Pang, H. J.; Tang, Q.; Wang, H. Y.; Chen, Y. G. *New J. Chem.* **2011**, *35*, 190. (b) Zhang, C. J.; Pang, H. J.; Tang, Q.; Wang, H. Y.; Chen, Y. G. *Dalton Trans.* **2010**, *39*, 7993. (c) Li, S.-L.; Lan, Y. Q.; Ma, J.-F.; Yang, J.; Wang, X. H.; Su, Z.-M. *Inorg. Chem.* **2007**, *46*, 8283.

(12) (a) Liu, H. Y.; Wu, H.; Ma, J.-F.; Song, S. Y.; Yang, J.; Liu, Y. Y.; Su, Z.-M. *Inorg. Chem.* **2007**, *46*, 7299. (b) Wu, H.; Dong, X. W.; Ma, J.-F.; Liu, H.-Y.; Yang, J.; Bai, H. Y. *Dalton Trans.* **2009**, 3162. (c) Bai, H. Y.; Yang, J.; Liu, B.; Ma, J.-F.; Kan, W. Q.; Liu, Y. Y.; Liu, Y. Y. *CrystEngComm* **2011**, *13*, 5877.

(13) (a) Liu, B.; Yu, Z. T.; Yang, J.; Wu, H.; Liu, Y. Y.; Ma, J.-F. *Inorg. Chem.* **2011**, *50*, 8967. (b) Wang, X.; Bi, Y.; Chen, B.; Lin, H.; Liu, G. *Inorg. Chem.* **2008**, *47*, 2442. (c) Lan, Y. Q.; Li, S.-L.; Shao, K.-Z.; Wang, X.-L.; Su, Z.-M. *Dalton Trans.* **2008**, 3824.

(14) (a) Xi, R.; Wang, B.; Isobe, K.; Nishioka, T.; Toriumi, K.; Ozawa, Y. *Inorg. Chem.* **1994**, *33*, 833. (b) Niu, Y. Y.; Wang, L. F.; Lv, X. R.; Du, H. J.; Qiao, Y. Z.; Wang, H. M.; Song, L. S.; Wu, B. L.; Hou, H. W.; Ng, S. W. *CrystEngComm* **2011**, *13*, 5071.

(15) (a) Gong, Y.; Zhou, Y. C.; Liu, T. F.; Lu, J.; Proserpio, D. M.; Cao, R. *Chem. Commun.* **2011**, *47*, 5982. (b) Carlucci, L.; Ciani, G.; Proserpio, D. M. *Coord. Chem. Rev.* **2003**, *246*, 247. (c) Abrahamas, B. F.; Batten, S. R.; Grannas, M. J.; Hamit, H.; Hoskins, B. F.; Robson, R. *Angew. Chem., Int. Ed.* **1999**, *38*, 1475. (d) Price, D. J.; Batten, S. R.; Moubaraki, B.; Murray, K. S. *Chem.—Eur. J.* **2000**, *6*, 3186. (e) Withersby, M. A.; Blake, A. J.; Champness, N. R.; Cooke, P. A.; Hubberstey, P.; Schroder, M. *J. Am. Chem. Soc.* **2000**, *122*, 4044.

(16) (a) Martin, D. P.; Supkowski, R. M.; LaDuca, R. L. *Inorg. Chem.* **2007**, *46*, 7917. (b) Wang, X. L.; Qin, C.; Wang, E. B.; Li, Y. G.; Su, Z.-M.; Xu, L.; Carlucci, L. *Angew. Chem., Int. Ed.* **2005**, *44*, 5824. (c) Montney, M. R.; Krishnan, S. M.; Patel, N. M.; Supkowski, R. M.; LaDuca, R. L. *Cryst. Growth Des.* **2007**, *7*, 1145. (d) Sun, J. K.; Yao, Q. X.; Ju, Z. F.; Zhang, J. *CrystEngComm* **2010**, *12*, 1709. (e) Zhan, S. Z.; Li, M.; Zhou, X. P.; Ni, J.; Huang, X. C.; Li, D. *Inorg. Chem.* **2011**, *50*, 8879.

(17) (a) Shyu, E.; Supkowski, R. M.; LaDuca, R. L. *Inorg. Chem.* **2009**, *48*, 2723. (b) Bi, M. H.; Li, G. H.; Hua, J.; Liu, X. M.; Hu, Y. W.; Shi, Z.; Feng, S. H. *CrystEngComm* **2007**, *9*, 984. (c) Tong, M. L.; Chen, X. M.; Batten, S. R. *J. Am. Chem. Soc.* **2003**, *125*, 16170. (d) Abrahams, B. F.; Batten, S. R.; Grannas, M. J.; Hamit, H.; Hoskins, B. F.; Robson, R. *Angew. Chem., Int. Ed.* **1999**, *38*, 1475. (e) Carlucci, L.; Ciani, G.; Proserpio, D. M.; Porta, F. *Angew. Chem., Int. Ed.* **2003**, *42*, 317.

(18) Zang, H. Y.; Du, D. Y.; Li, S.-L.; Lan, Y. Q.; Yang, G. S.; Yan, L. K.; Shao, K. Z.; Su, Z.-M. *J. Solid State Chem.* **2011**, *184*, 1141.

(19) Liu, H. Y.; Liu, B.; Yang, J.; Liu, Y. Y.; Ma, J.-F.; Wu, H. *Dalton Trans.* **2011**, *40*, 9782.

(20) (a) Hagrman, D.; Zubieta, C.; Rose, D. J.; Zubieta, J.; Haushalter, R. C. *Angew. Chem., Int. Ed.* **1997**, *36*, 873. (b) Zhang, X.; Wei, P.; Sun, D.; Ni, Z.; Dou, J.; Li, B.; Shi, C.; Hu, B. *Cryst. Growth Des.* **2009**, *9*, 4424.

(21) Kan, W. Q.; Ma, J.-F.; Liu, Y. Y.; Wu, H.; Yang, J. *CrystEngComm* **2011**, *13*, 7037.

(22) (a) Dessapt, R.; Kervern, D.; Bujoli-Doeuff, M.; Deniard, P.; Evain, M.; Jobic, S. *Inorg. Chem.* **2010**, *49*, 11309. (b) Coué, V.; Dessapt, R.; Bujoli-Doeuff, M.; Evain, M.; Jobic, S. *J. Solid State Chem.* **2006**, *179*, 3615. (c) Wang, X. J.; Kang, B. S.; Su, C. Y.; Yu, K. B.; Zhang, H. X.; Chen, Z. N. *Polyhedron* **1999**, *18*, 3371.

(23) Zhang, C. J.; Pang, H. J.; Tang, Q.; Wang, H. Y.; Chen, Y. G. *New J. Chem.* **2011**, *35*, 190.
(24) (a) Zhai, Q. G.; Wu, X. Y.; Chen, S. M.; Zhao, Z. G.; Lu, C. Z. *Inorg. Chem.* **2007**, *46*, 5046. (b) Liao, J. H.; Huang, J. S.; Lai, Y. C. *Cryst. Growth Des.* **2006**, *6*, 354.
(25) (a) Wu, H.; Liu, H. Y.; Liu, B.; Yang, J.; Liu, Y. Y.; Ma, J.-F.; Liu, Y. Y.; Bai, H. Y. *CrystEngComm* **2011**, *13*, 3402. (b) Zheng, X. J.; Jin, L. P.; Gao, S.; Lu, S. Z. *New J. Chem.* **2005**, *29*, 798. (c) Yang, J.; Yue, Q.; Li, G. D.; Cao, J. J.; Li, G. H.; Chen, J. S. *Inorg. Chem.* **2006**, *45*, 2857. (d) Bai, H. Y.; Ma, J.-F.; Yang, J.; Liu, Y. Y.; Wu, H.; Ma, J. C. *Cryst. Growth Des.* **2010**, *10*, 995. (e) Wu, H.; Liu, H. Y.; Yang, J.; Liu, B.; Ma., J.-F.; Liu, Y. Y.; Liu, Y. Y. *Cryst. Growth Des.* **2011**, *11*, 2317.
(26) (a) Wu, H.; Liu, H.-Y.; Liu, Y.-Y.; Yang, J.; Liu, B.; Ma, J.-F. *Chem. Commun.* **2011**, *47*, 1818. (b) Chen, Z. L.; Su, Y.; Xiong, W.; Wang, L. X.; Liang, F. P.; Shao, M. *CrystEngComm* **2009**, *11*, 318. (c) Zhang, L. Y.; Zhang, J. P.; Lin, Y. Y.; Chen, X. M. *Cryst. Growth Des.* **2006**, *6*, 1684. (d) Chu, Q.; Liu, G. X.; Huang, Y. Q.; Wang, X. F.; Sun, W. Y. *Dalton Trans.* **2007**, 4302. (e) Wang, X.-L.; Qin, C.; Wang, E. B.; Li, Y. G.; Hao, N.; Hu, C. W.; Xu, L. *Inorg. Chem.* **2004**, *43*, 1850. (f) Kan, W. Q.; Liu, Y. Y.; Yang, J.; Liu, Y. Y.; Ma, J.-F. *CrystEngComm* **2011**, *13*, 4256.
(27) (a) Thirumurugan, A.; Natarajan, S. *Dalton Trans.* **2004**, 2923. (b) Zhang, L. P.; Ma, J.-F.; Yang, J.; Liu, Y. Y.; Wei, G. H. *Cryst. Growth Des.* **2009**, *9*, 4660.
(28) Li, H. X.; Zhang, X. Y.; Huo, Y. N.; Zhu, J. *Environ. Sci. Technol.* **2007**, *41*, 4410.
(29) (a) Tsumura, T.; Kojitan, N.; Izumi, I.; Iwashita, N.; Toyoda, M.; Inagaki, M. *J. Mater. Chem.* **2002**, *12*, 1391. (b) Muggli, D. S.; Ding, L.; Odland, M. *J. Catal. Lett.* **2002**, *78*, 23. (c) Asahi, R.; Morikawa, T.; Ohwaki, T.; Aoki, K.; Taga, Y. *Science* **2001**, *293*, 269. (d) Lin, H.; Maggard, P. A. *Cryst. Growth Des.* **2010**, *10*, 1323.
(30) Wang, C.; Xie, Z.; deKrafft, K. E.; Lin, W. *Appl. Mater. Interfaces* **2012**, *4*, 2288.
(31) Zeng, H.; Liu, P.; Cai, W.; Yang, S.; Xu, X. *J. Phys. Chem. C* **2008**, *112*, 19620.
(32) (a) Liu, H.-Y.; Wu, H.; Ma, J.-F.; Liu, Y.-Y.; Yang, J.; Ma, J. C. *Dalton Trans.* **2011**, *40*, 602. (b) Wang, B.; Dong, S. *Electrochim. Acta* **1992**, *37*, 1859. (c) Dong, S.; Wang, B. *Electrochim. Acta* **1992**, *37*, 11. (d) Wang, P.; Wang, X. P.; Zhu, G. Y. *Electrochim. Acta* **2001**, *46*, 637.
(33) Lan, Y. Q.; Li, S.-L.; Shao, K.-Z.; Wang, X.-L.; Hao, X.-R.; Su, Z.-M. *Dalton Trans.* **2009**, 940.
(34) (a) Han, Z. G.; Zhao, Y. L.; Peng, J.; Liu, Q.; Wang, E. B. *Electrochim. Acta* **2005**, *51*, 218. (b) Wang, X.-L.; Wang, E. B.; Lan, Y.; Hu, C. W. *Electroanalysis* **2002**, *14*, 1116. (c) Zhu, M.; Peng, J.; Pang, H. J.; Zhang, P. P.; Chen, Y.; Wang, D. D.; Liu, M. G.; Wang, Y. H. *Inorg. Chim. Acta* **2010**, *363*, 3832.